© 2014. Published by The Company of Biologists Ltd | Development (2014) 141, 4489-4499 doi:10.1242/dev.107193

RESEARCH ARTICLE

Excessive vascular sprouting underlies cerebral hemorrhage in mice lacking αVβ8-TGFβ signaling in the brain

Thomas D. Arnold[1,2,*,§§], Colin Niaudet[2,‡,‡‡], Mei-Fong Pang[2,§,‡‡], Julie Siegenthaler[3,¶], Konstantin Gaengel[2,‡], Bongnam Jung[2,‡], Gina M. Ferrero[4], Yoh-suke Mukouyama[5], Jonas Fuxe[2], Rosemary Akhurst[6], Christer Betsholtz[2,‡], Dean Sheppard[7] and Louis F. Reichardt[4,,§§]**

ABSTRACT

Vascular development of the central nervous system and blood-brain barrier (BBB) induction are closely linked processes. The role of factors that promote endothelial sprouting and vascular leak, such as vascular endothelial growth factor A, are well described, but the factors that suppress angiogenic sprouting and their impact on the BBB are poorly understood. Here, we show that integrin αVβ8 activates angiosuppressive TGFβ gradients in the brain, which inhibit endothelial cell sprouting. Loss of αVβ8 in the brain or downstream TGFβ1-TGFBR2-ALK5-Smad3 signaling in endothelial cells increases vascular sprouting, branching and proliferation, leading to vascular dysplasia and hemorrhage. Importantly, BBB function in *Itgb8* mutants is intact during early stages of vascular dysgenesis before hemorrhage. By contrast, *Pdgfb*$^{ret/ret}$ mice, which exhibit severe BBB disruption and vascular leak due to pericyte deficiency, have comparatively normal vascular morphogenesis and do not exhibit brain hemorrhage. Our data therefore suggest that abnormal vascular sprouting and patterning, not BBB dysfunction, underlie developmental cerebral hemorrhage.

KEY WORDS: Angiogenesis, Brain, CNS, Hemorrhage, Sprouting, Integrin αVβ8, TGFβ, Mouse

INTRODUCTION

In angiogenesis, new blood vessels form from pre-existing ones in an iterative sprouting and branching process (Blanco and Gerhardt, 2013). Angiogenesis is the principal mode of vascular development in the central nervous system (CNS). In the CNS, capillaries sprout from perineural vessels, invade the neuroepithelium and form functional vessels by branching and anastamosis of neighboring sprouts (Ballabh et al., 2004a; Vasudevan et al., 2008; Walls et al., 2008). As they grow, nascent sprouts extend filopodia toward sources of VEGF (James et al., 2009; Ruhrberg et al., 2002), and are specified into tip and stalk cells by Dll4/Notch-mediated lateral inhibition (Phng and Gerhardt, 2009). Initial sprouting and patterning is further regulated by signaling systems, including netrin (Freitas et al., 2008), ephrin (Sawamiphak et al., 2010; Wang et al., 2010), BMP (Kim et al., 2012; Larrivée et al., 2012; Moya et al., 2012), Wnt/β-Catenin (Corada et al., 2010; Gore et al., 2011) and angiopoietin (Fagiani and Christofori, 2013). Once primary CNS angiogenesis is complete, sprouting angiogenesis is suppressed and new vessels are stabilized (Gaengel et al., 2012; Jung et al., 2012; Shoham et al., 2012). During angiogenesis, mural cells provide additional structural support and regulate vascular permeability (Armulik et al., 2005; Daneman et al., 2010; Hellström et al., 2001). Compared with angiogenic growth, angiogenic suppression and vessel maturation are not well understood, although recent studies support an important role for S1P/S1PR1 signaling (Gaengel et al., 2012; Jung et al., 2012; Liu et al., 2000; Shoham et al., 2012).

Prior studies from ours and other laboratories have described defects in brain vascular development following neuroepithelial cell-specific deletion of the integrin αVβ8 (McCarty et al., 2005; Proctor et al., 2005). As the αVβ8 integrin has been shown to mediate TGFβ activation *in vitro* (Cambier et al., 2005), this suggested that αVβ8 on neuroepithelial cells activates TGFβ, which subsequently promotes vascular integrity. The similarities in phenotype of neuroepithelial-specific *Itgav* and *Itgb8* mutants with endothelial-specific mutations of *Tgfbr2* (Robson et al., 2010), *Alk5* (Nguyen et al., 2011) and *Smad2/Smad3* (Itoh et al., 2012) support this proposal. In each mutant, vessels were 'stalled' in their growth from the pia mater towards the ventricle. However, one study reports a lack of major vascular phenotypes in endothelial cell-specific mutants of *Tgfbr2* and *Alk5* (Park et al., 2008), leaving uncertain the cell types through which αVβ8 regulates brain angiogenesis.

Most existing literature suggests that intracerebral hemorrhage during brain development results from increased vascular permeability and a defective blood-brain barrier (BBB) (Ballabh et al., 2004b). These studies, however, have not determined whether vascular permeability was elevated before initial hemorrhage.

In this study, we monitored the appearance of angiogenic defects in neuroepithelial-specific αVβ8 and TGFβ signaling pathway mutants, with the aim of understanding how disruption in this pathway results in vascular malformation and hemorrhage. By contrast to prior studies, we did not observe defects in vascular ingress into the developing brain. Our data show that αVβ8 activates TGFβ in a ventral-dorsal gradient in the brain, and that TGFβ1 signaling in endothelial cells (via TGFBR2-ALK5-Smad3) suppresses angiogenic sprouting and promotes vascular stability. When signaling is disrupted, vessels excessively sprout and branch, and eventually coalesce into dysplastic, glomeruloid

[1]Department of Pediatrics, University of California, San Francisco, San Francisco, CA 94158, USA. [2]Department of Medical Biochemistry and Biophysics, Karolinska Institutet, SE-177 77 Stockholm, Sweden. [3]Department of Neurology, University of California, San Francisco, San Francisco, CA 94158, USA. [4]Department of Physiology and Neuroscience Program, University of California, San Francisco, San Francisco, CA 94158, USA. [5]Laboratory of Stem Cell and Neuro-Vascular Biology, National Heart, Lung, and Blood Institute, NIH, Bethesda, MD 20892, USA. [6]Helen Diller Cancer Center and Department of Anatomy, University of California, San Francisco, San Francisco, CA 94158, USA. [7]Department of Medicine, University of California, San Francisco, San Francisco, CA 94158, USA.
*Present address: Department of Pediatrics, University of California, San Francisco, San Francisco, CA 94158, USA. ‡Present address: Department of Immunology, Genetics and Pathology, Uppsala University, SE-751 85 Uppsala, Sweden. §Present address: Department of Chemical and Biological Engineering, Princeton University, Princeton, NJ 08544, USA. ¶Present address: Department of Pediatrics, Denver-Anschutz Medical Campus, University of Colorado, Aurora, CO 80045, USA. **Present address: Simons Foundation, 160 Fifth Avenue, New York, NY 10010, USA.
‡‡These authors contributed equally to this work

§§Authors for correspondence (arnoldtd@gmail.com; LReichardt@simonsfoundation.org)

Received 21 December 2013; Accepted 1 September 2014

Development (2014) 141, 4489-4499 doi:10.1242/dev.107193

vessels. Importantly, increased vascular permeability does not precede hemorrhage. We propose a model for graded activation of TGFβ by αVβ8 in the CNS, which suppresses sprouting angiogenesis, thereby stabilizing blood vessels.

RESULTS

Hemorrhage, but not BBB dysfunction, is associated with vascular dysplasia in *Itgb8ΔNE* mutants

We previously showed that global (*Itgb8*$^{-/-}$) and neuroepithelial-specific (*Itgb8ΔNE*) deletion of *Itgb8* resulted in abnormal vessel growth and hemorrhage in the embryonic forebrain. Vessels 'stalled' before reaching the cerebral ventricle, and 'failed to form an organized anastomotic network' (McCarty et al., 2002, 2005; Proctor et al., 2005; Zhu et al., 2002). To better understand the causes of vascular malformation and hemorrhage in *Itgb8ΔNE* mutants, we re-analyzed these phenotypes in more detail. In contrast to previous reports (McCarty et al., 2002, 2005; Proctor et al., 2005; Zhu et al., 2002), we found that initial blood vessel ingression proceeded normally in *Itgb8ΔNE* mutants. In both mutants and controls, vessels migrated from the perineural vascular plexus (PNVP) into the ventral forebrain and formed a periventricular vascular plexus (PVP) (Fig. 1A) by E10.5. Normally, the PVP extends in a ventral to dorsal fashion, iteratively creating vascular loops with the PNVP (Takashima and Tanaka, 1978; Vasudevan et al., 2008; Walls et al., 2008; Yu et al., 1994). Compared with controls, the ventral-to-dorsal extension of the PVP over time was not impaired in mutants (see yellow arrows in Fig. 1A, E10.5-E12.5). As previously reported, we observed subtle vascular irregularities, predominantly in the ventral regions of the brain, beginning at E11.5 (Fig. 1A,B). Vascular dysplasia became more noticeable at E12.5, when vessels formed abnormal glomeruloid bodies (Fig. 1A,B, double arrowheads). These malformations occurred first in the ventral forebrain, then subsequently in more dorsal regions. Interestingly, hemorrhage was spatially and temporally linked with PVP vascular malformations: hemorrhage always occurred initially in the ventral forebrain near the ventricular surface adjacent to glomeruloid malformations, and progressed dorsally (Fig. 1A). This ventral-to-dorsal pattern of vascular ingression, followed by PVP dysplasia and hemorrhage, was also evident in the spinal cord, hindbrain and cerebellum (supplementary material Fig. S1). By contrast, in the peripheral nervous system, vascular patterning, endothelial cell differentiation and nerve-vessel alignment were normal, with no hemorrhage (supplementary material Fig. S1).

Numerous mutants exhibit intracerebral hemorrhage and associated vascular dysplasia. Hemorrhage has generally been attributed to a dysfunctional BBB (Cullen et al., 2011; Liebner et al., 2008; Mobley et al., 2009; Nguyen et al., 2011; Stenman et al., 2008). Other mutants, however, develop vascular leak without hemorrhage (Armulik et al., 2010; Bell et al., 2010; Daneman et al., 2010; Nitta et al., 2003; Wang et al., 2012), suggesting that these are distinct processes. To test the

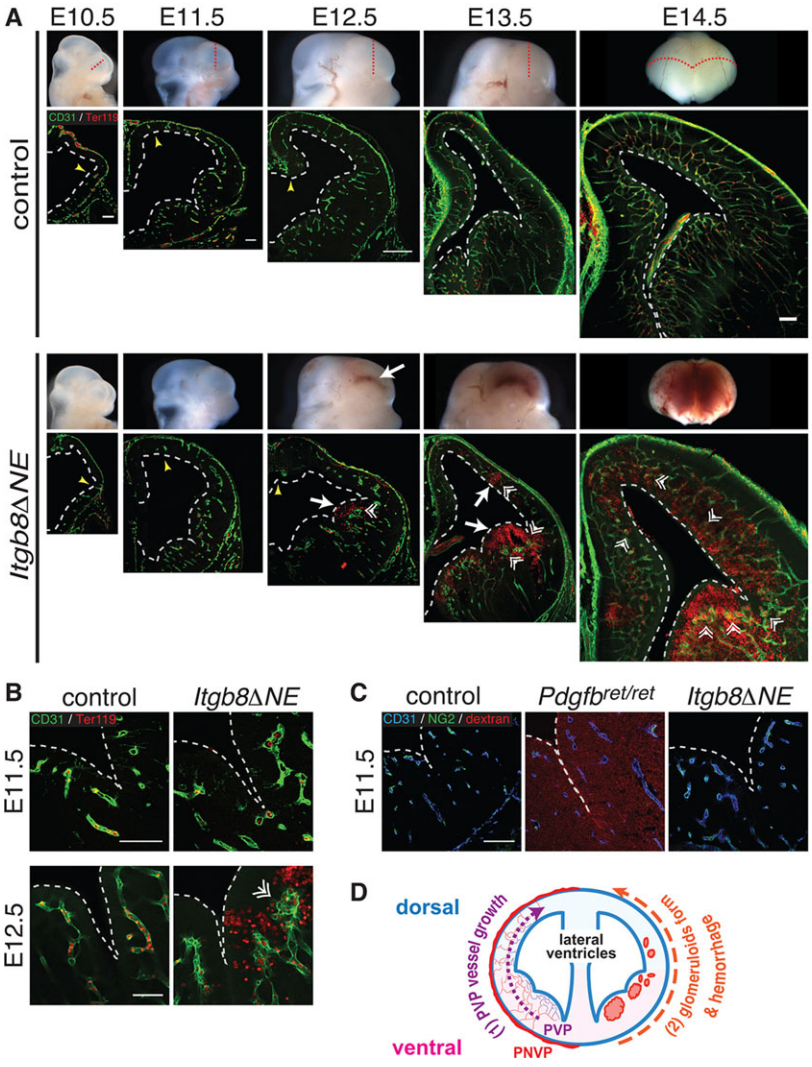

Fig. 1. Vascular dysplasia and hemorrhage in brains of neuroepithelial-specific *Itgb8* (*Itgb8ΔNE*) mutants. (A) Coronal sections (dotted red lines) of E10.5-E14.5 brains with labeling of endothelial (CD31, green) and red blood cells (Ter119, red). (B) Higher magnification images at E11.5 and E12.5. At E10.5, pia-associated vessels outside the CNS (PNVP) surround the developing forebrain in control and mutant. Yellow arrowheads at E10.5-E12.5 indicate the dorsal limits of neuroepithelium invasion by the PVP. Initial PVP formation and dorsal invasion occur normally in mutants. At E11.5, PVP vessels appear thicker and more tortuous in mutants versus controls. In mutants, hemorrhage (white arrows) is first observed ventrally at E12.5 and later in more dorsal regions (E13.5, E14.5). Also, note enlargement of the lateral ventricles (dashed white lines) in mutants versus controls. At E12.5 in the ventral telencephalon, the mutant vasculature forms large glomeruloid malformations (double arrowheads) near sites of hemorrhage. At E13.5 and E14.5, similar malformations are observed in the dorsal telencephalon coincident with hemorrhage. *N*>4. (C) Vascular barrier function is intact before hemorrhage in *Itgb8ΔNE* embryos following trans-cardiac perfusion of 70 kDa dextran-TMR tracer (CD31-endothelium, blue; NG2-pericytes, green) and tracer (red). Pericyte-deficient *Pdgfb*$^{ret/ret}$ mice (middle panel) provided a positive control. *N*>4. Scale bars: 250 µm. (D) Diagram illustrating PVP development: (1) PVP vessels ingress from the PNVP to the subventricular zone and then expand dorsally over time (2) in association with glomeruloid malformation and hemorrhage appearance in mutants.

Development (2014) 141, 4489-4499 doi:10.1242/dev.107193

role of neuroepithelial *Itgb8* in maintaining the BBB, we injected a fluorescent tracer into the cardiac outflow tracts of control and mutant embryos at E11.5, when there were mild vessel irregularities, but one day before detectable hemorrhage. Pericyte-deficient *Pdgfb*$^{ret/ret}$ mice (Armulik et al., 2010), which lack a functional BBB, served as a positive control for vascular leak. We found that *Pdgfb*$^{ret/ret}$ mice exhibit diffuse leakage of the 70 kDa dextran tracer but lack obvious hemorrhage (Fig. 1C, Fig. 3E). By contrast, no detectable leakage was observed in controls or *Itgb8ΔNE* mutants (Fig. 1C), although they subsequently developed severe hemorrhage (Fig. 1A,B). Thus, at E11.5 a functional BBB exists in *Itgb8ΔNE* mutants. Taken together, our observations indicate that BBB dysfunction does not explain the appearance of intracerebral hemorrhage in *Itgb8ΔNE* mice.

Vascular hypersprouting/hyperbranching precedes glomeruloid formation and hemorrhage in *Itgb8ΔNE* mutants

The coincidence of hemorrhage with glomeruloid malformations, and the absence of vascular leak before hemorrhage, suggested to us that abnormal blood vessel formation might result in hemorrhage in *Itgb8ΔNE* mutants. To directly assess changes in angiogenic sprouting and branching due to loss of *Itgb8*, we labeled the vasculature in whole telencephalons, using anti-CD31 or anti-collagen IV antibodies, and imaged neuroepithelial flat-mounts at various depths (schematic, Fig. 2). In this way, the telencephalic vasculature has a stereotyped architecture which develops in a spatial-temporal sequence (Fig. 2): parent vessels in the PNVP (level 4) give rise to smaller radial vessels (level 3), which penetrate the neuroepithelium and connect to a planar capillary bed adjacent to the ventricle (PVP, level 2). Filopodia extend from tip cells towards adjacent PVP vessels (level 2), as well as the ventricular surface (level 1, and supplementary material Movie 1). Angiogenesis is initiated and proceeds in a ventral-to-dorsal gradient, with greater vascular density, branch points and filopodia in ventral regions, and a progressive increase in their densities from E11.5 until ~E14.5 (Fig. 2B,C; supplementary material Fig. S2), after which vascular growth slows compared with ongoing neuroepithelial expansion. A similar patterning gradient is also observed in the hindbrain (supplementary material Fig. S3). Comparing *Itgb8ΔNE* mutants with littermate controls, we did not observe differences in PNVP vessel appearance or radial vessel numbers leading to the PVP [Fig. 2B (level 4 and 3) and 2C]. However, the mutant PVP contained a greater vascular density with more branches and more filopodia extending toward the ventricular surface [Fig. 2B (level 2 and 1) and 2C; supplementary material Movies 1 and 2]. Associated with these increases, endothelial cell proliferation in the ventral PVP was also significantly increased in E11.5 mutants (Fig. 1C; supplementary material Fig. S4). Increased sprouting and branching was most pronounced in the ventral telencephalon, but was observed elsewhere in the CNS (see supplementary material Fig. S3), and progressed from E11.5 to E12.5 (Fig. 2C; supplementary material Fig. S3). In summary, these results demonstrate hypersprouting/hyperbranching of the PVP in mutants. Importantly, the ventral-dorsal progression of angiogenic abnormalities immediately precedes, and might therefore

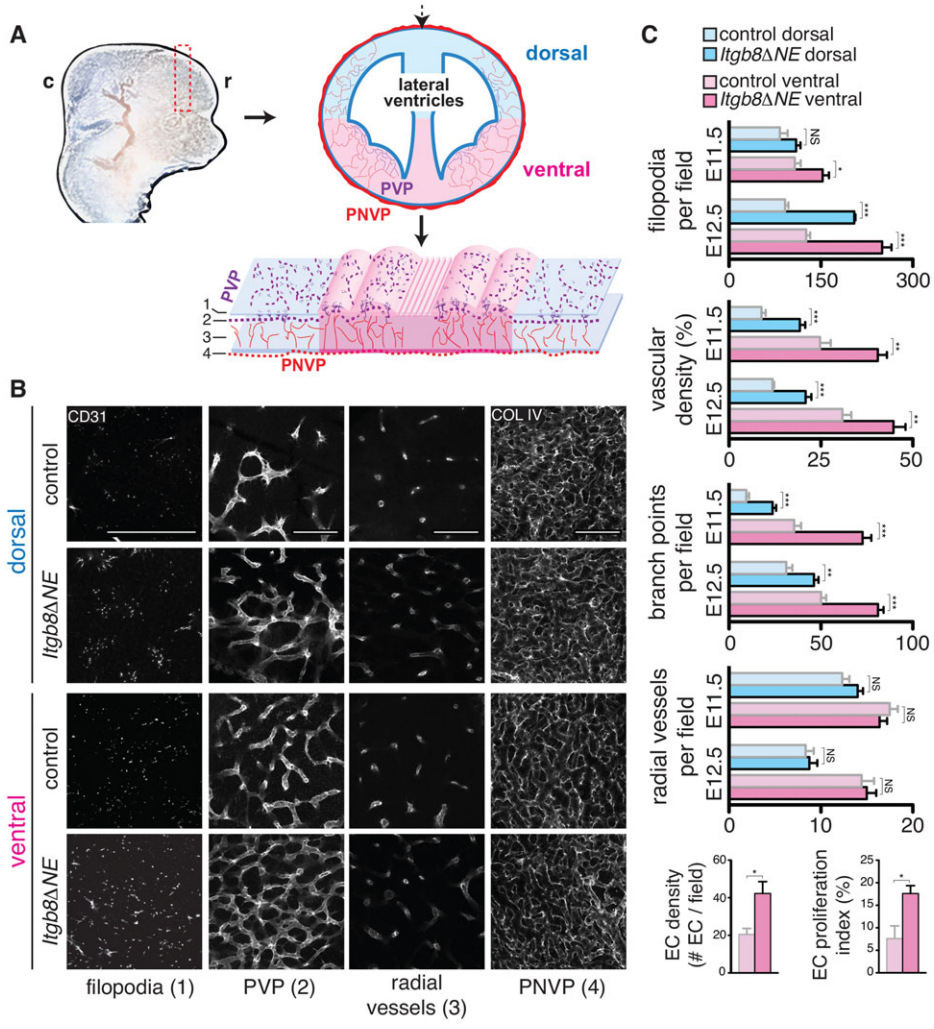

Fig. 2. Increased vascular sprouting and branching before hemorrhage in *Itgb8ΔNE* mutants. (A) Diagram illustrating neuroepithelial flat-mounts used to analyze vascular sprouting and branching in the telencephalon. c, caudal; r, rostral. (B) E11.5 coronal sections (dashed red rectangle in A) were immunostained, cut dorsally (dashed black arrow in A) and flattened. Vessels were visualized at depths (1-4) indicated in bottom panel of A: (1) vascular filopodia extending to the ventricular surface, (2) PVP in the subventricular zone, (3) radial sprouts from the PNVP leading to PVP vessels and (4) pia-associated PNVP. Images illustrate increased densities of endothelial cell filopodia, vascular branch points and total vascular coverage in mutants versus controls (see supplementary material Movies 1 and 2). The number of radial sprouts (3) and the appearance/organization of the PNVP (4) appear similar in both. Scale bars: 100 µm. (C) Quantitative analysis of E11.5 and E12.5 flat-mounts (images not shown): filopodia number/field, vascular density, vessel branch points/field, radial vessels connecting PNVP to PVP per field. Endothelial cell number (Erg$^+$ endothelial nuclei per 100 µm vascular length) and endothelial proliferation index (percentage of Erg$^+$ nuclei labeled by BrdU; see supplementary material Fig. S2). Quantification reveals spatio-temporal PVP sprouting and branching angiogenesis gradients in controls with increased vascular sprouting, and branching and endothelial proliferation in mutants before and with hemorrhage. *P*-values from Student's *t*-test: **P*<0.05, ***P*<0.005, ****P*<0.0005; NS, not significant. *N*=4 controls, four mutants per time point. Error bars indicate s.e.m.

Development (2014) 141, 4489-4499 doi:10.1242/dev.107193

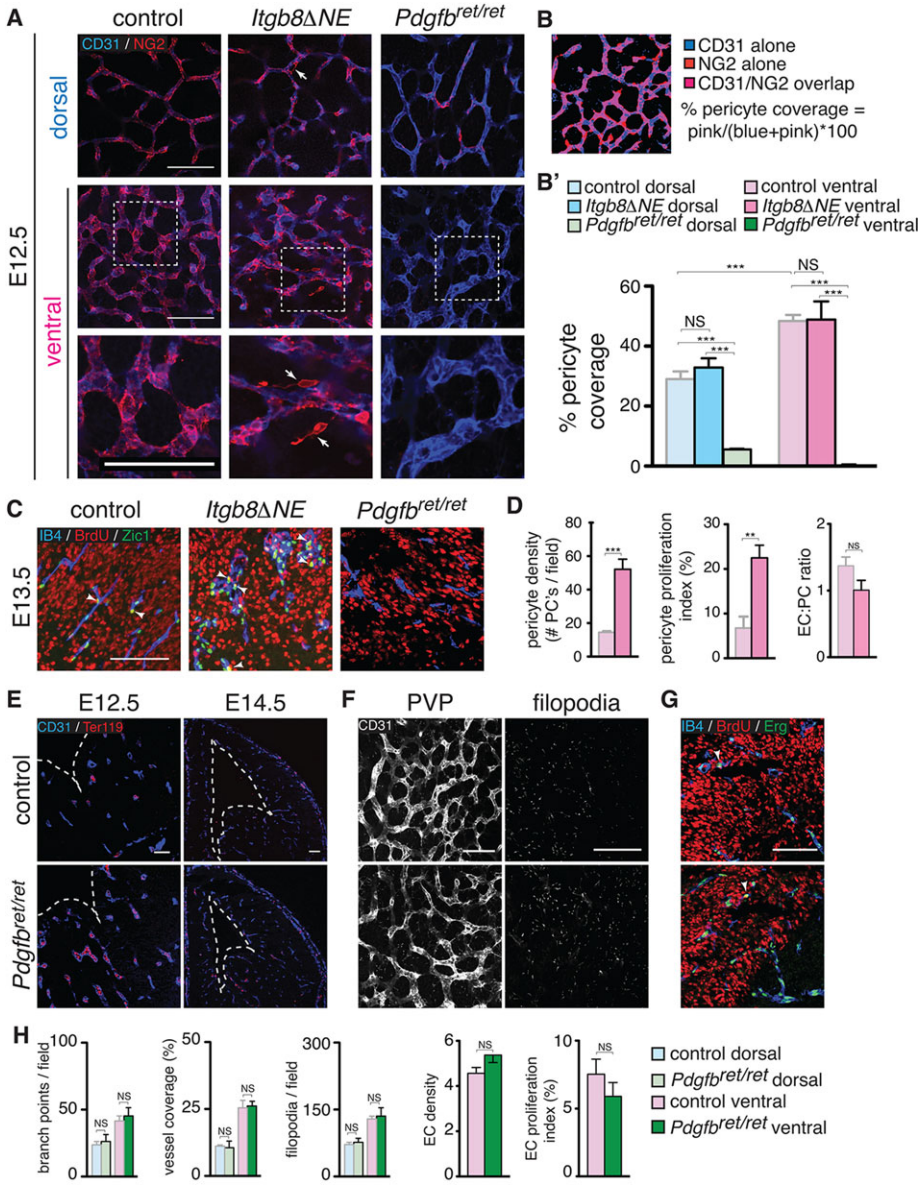

Fig. 3. Pericyte density, proliferation and detachment co-incident with hemorrhage in *Itgb8ΔNE* mutants. (A) Endothelium (CD31, blue) and pericyte (NG2, red) staining of dorsal and ventral PVPs in E12.5 mutants and littermate control flat-mounts. Pericyte coverage in dorsal and ventral regions is similar in mutants versus controls with significantly higher coverage in ventral regions. Higher magnification insets are indicated by dashed boxes in center panels and are shown in bottom panels. They depict pericyte detachment from the endothelium in mutants (arrows). *Pdgfb*$^{ret/ret}$ mutants (which lack pericytes) provided a negative control. (B) Example of data and method used to quantify pericyte coverage (see Materials and Methods). (B′) Quantitative assessment of pericyte coverage in control, *Itgb8ΔNE* and *Pdgfb*$^{ret/ret}$ telencephalon at E12.5. *N*=4 for each genotype. (C) Quantification of pericyte proliferation at 2 h. BrdU pulse. Proliferating cells (BrdU, red), endothelia (isolectin B4, blue) and pericytes (Zic1, green). Arrowheads depict BrdU/Zic1 double-positive cells. (D) Quantitation of pericyte density, proliferation and endothelial:pericyte cell ratio in control and mutants. *Pdgfb*$^{ret/ret}$ mutant mice (no pericytes in ventral forebrain at this time point) provide a negative control. Pericyte density, proliferation and detachment appear normal in the mutant at time points before hemorrhage (not shown). *N*=4 controls, 4 mutants. (E) Absence of hemorrhage in *Pdgfb*$^{ret/ret}$ mutants at E12.5 and E14.5 [vascular endothelial cells (anti-CD31, blue); red blood cells (Ter119, red)]. (F) Flat-mounts from E12.5 *Pdgfb*$^{ret/ret}$ mice with endothelial cells (CD31, white) imaged at the PVP and filopodia levels (levels 2 and 1, respectively, of Fig. 2 diagram) reveal comparatively normal angiogenic patterning and filopodial extension in pericyte-deficient mice. (G) Co-staining for BrdU and Erg reveals no difference in endothelial cell number or proliferation in E12.5 *Pdgfb*$^{ret/ret}$ mutants. (H) Quantitation of angiogenesis at E12.5 indicates that endothelial cell, vascular branch point and filopodial densities are similar in controls and *Pdgfb*$^{ret/ret}$ mutants. Vascular coverage and endothelial cell proliferation are also normal in mutants. *N*=4 controls, 4 mutants. *P*-values from Student's *t*-test: ***P*<0.005, ****P*<0.0005; NS, not significant. Error bars indicate s.e.m. Scale bars: 100 µm.

cause, the formation of overtly dysplastic vessels and hemorrhage, which occur in the same pattern, one day later.

Pericyte proliferation in *Itgb8ΔNE* embryos

Pericytes have well-described roles in vascular development and formation of the BBB (Armulik et al., 2010; Bell et al., 2010; Daneman et al., 2010; Hellström et al., 2001), and recent studies invoke pericyte deficiency as a potential cause of brain hemorrhage (Braun et al., 2007; Li et al., 2011). Using telencephalic flat-mounts we quantified brain pericyte coverage, density and proliferation at E12.5, using pericyte-deficient *Pdgfb*$^{ret/ret}$ mice for comparison. In contrast to previous studies using humans and rabbits, which reported a relative paucity of pericytes in ventral brain regions (Braun et al., 2007), we found that pericyte coverage at approximately

Development (2014) 141, 4489-4499 doi:10.1242/dev.107193

equivalent developmental stages in mice was greater in ventral than in dorsal brain regions (Fig. 3A,B′; pericyte coverage and number in *Pdgfb*$^{ret/ret}$ mutants were negligible). Additionally, we found no difference in pericyte coverage in either ventral or dorsal domains between control and *Itgb8* mutants. Interestingly, in the mutant, we observed occasional NG2^{+} pericytes detached from the vasculature (arrows in Fig. 3). We also observed significant increases in pericyte density (pericyte-specific Zic1^{+} nuclei) and proliferation (BrdU incorporation) in mutants (Fig. 3C,D). However, the endothelial cell-to-pericyte (EC:PC) ratio was not significantly different from controls at E12.5 (Fig. 3D). Also, on E11.5, one day before the appearance of hemorrhage, there was no significant difference in pericyte density or proliferation (not shown). Taken together, it seems likely that pericyte proliferation is a secondary consequence of increased endothelial proliferation.

The absence of any defect in pericyte number or coverage before cerebral hemorrhage in *Itgb8ΔNE* mutants prompted us to evaluate the purported association between reduced pericyte coverage and brain hemorrhage (Braun et al., 2007; Li et al., 2011). Surprisingly, there was no detectable hemorrhage at E12.5 or E14.5 in pericyte-deficient *Pdgfb*$^{ret/ret}$ mice (Fig. 3E), despite diffuse vascular leak in these mutants at E11.5 (Fig. 1B). Thus, vascular leak does not invariably result in hemorrhage. Because vascular hypersprouting/hyperbranching and elevated endothelial cell proliferation preceded the development of vascular malformation and hemorrhage in *Itgb8ΔNE* mice, we analyzed these parameters in *Pdgfb*$^{ret/ret}$ mutants. In contrast to the integrin mutant, vascular branching and endothelial cell proliferation were not significantly elevated in the *Pdgfb*$^{ret/ret}$ mutant (Fig. 3F-H). Taken together, these data suggest that abnormal angiogenesis and/or vascular malformation are required for hemorrhage.

Loss of active TGFβ1 and reduced phospho-Smad3 in endothelial cells in the *Itgb8ΔNE* mutant CNS

CNS angiogenesis is regulated by a balance between angiogenic and angiosuppressive signals, including VEGF, bFGF, sFLT1, S1P and TGFβ/BMP. We and others have shown that astroglial αVβ8 binds to and activates TGFβ1 and TGFβ3 (Cambier et al., 2005; Melton et al., 2010; Yang et al., 2007). Deletion of *Itgb8* in retinal Muller glia reduces paracrine TGFβ signaling in retinal endothelia, causing hyperbranching (Allinson et al., 2012; Arnold et al., 2012; Hirota et al., 2011). Little is known, however, about the regional activation of TGFβ ligand by αVβ8 in the developing brain, and the consequences of altered TGFβ activation on sprouting angiogenesis. We therefore labeled the ventricular surface of whole-mount E11.5 mutant and controls with an antibody recognizing activated TGFβ1/3 (Yamazaki et al., 2011). Results revealed that the highest concentration of activated TGFβ was in the ventral/midline and decreased in a gradient toward dorsal/lateral brain regions (Fig. 4A, left). In the absence of *Itgb8*, there were dramatic reductions in TGFβ concentration and absence of an obvious gradient, with small amounts of residual peri-vascular anti-active TGFβ (Fig. 4A, right, schematic).

These results argue that αVβ8 probably controls angiogenesis through activation of TGFβ. We next sought to identify the major αVβ8- and TGFβ-regulated intracellular signaling pathway controlling angiogenic responses. TGFβ acts through complexes of type I and type II receptors that promote Smad transcription factor phosphorylation. TGFBR1/ALK5 with TGFBR2 induces phosphorylation of Smad2/3 complexes. In endothelial cells, an alternative type I receptor, ALK1, is thought to complex with BMPR2 to induce phosphorylation of Smad1/5/8, which interact with Notch effectors to promote stalk cell differentiation (Kim et al., 2012; Larrivée et al., 2012; Li et al., 2011; Moya et al., 2012). Although BMP9 and BMP10 are believed to be the major ALK1 ligands, TGFβ can activate ALK5-TGFBR2 (Smad2/3) and ALK1-BMPR2 (Smad1/5/8) *in vitro*, and in certain contexts *in vivo* (Pardali et al., 2010). To determine which pathways are activated during brain vascular development, we analyzed the location and relative abundance of C-terminally phosphorylated (p)Smad3 and Smad1/5/8 proteins in telencephalic brain sections from E11.5 *Itgb8* mutants and controls. Nuclear pSmad3 staining in controls was ubiquitous, with high-intensity staining in blood vessels (pericytes and endothelial tip and stalk cells) and relatively low-intensity staining in subventricular zone neuroepithelial cells (Fig. 4B). Nuclear pSmad3 was significantly reduced in telencephalic PVP vessels of *Itgb8ΔNE* mice, as evidenced by reduced pSmad3 staining intensity in IB4-labeled vessels (Fig. 4B,C). Next, we analyzed nuclear pSmad1/5/8 protein in controls and mutants. Consistent with recent reports (Falk et al., 2008; Moya et al., 2012), we observed intense pSmad1/5/8 staining in endothelial cells (tip and stalk cells) and less intense staining in subventricular zone neuroepithelial cells (Fig. 4B′). In contrast to pSmad3, fluorescence intensity mapping and quantification revealed no change in vascular pSmad1/5/8 signaling in the *Itgb8ΔNE* brain (Fig. 4B′,C). Consistent with elevated endothelial proliferation (Fig. 2C), we observed significantly more vascular nuclei per vessel length in *Itgb8ΔNE* mutants (Fig. 4B,C). These data indicate that αVβ8-activated TGFβ primarily controls activation of Smad3, not Smad1/5/8. The presence of significant levels of pSmad1/5/8 in the *Itgb8ΔNE* brain suggests that Smad1/5/8-regulated pathways cannot compensate effectively for loss of pSmad3 in CNS endothelial cells.

To evaluate the direct effects of TGFβ on sprouting, we used a previously described cell culture system (Gaengel et al., 2012) in which mouse MS-1 microvascular endothelial cells seeded on beads are allowed to sprout in fibrin gels. Similar to previous reports (Liu et al., 2009), we found that addition of TGFβ suppresses, whereas inhibition of ALK5 greatly enhances sprouting (Fig. 4D,E). Consistent with our *in vivo* results, blocking Smad3 activity using Specific Inhibitor of Smad3 (SIS3) (Jinnin et al., 2006; Li et al., 2010) enhanced endothelial cell sprouting to a similar degree as the more general ALK5 inhibitor SB431542 (Fig. 4D,E). Taken together, these data indicate that the αVβ8-TGFβ-TGFBR2-ALK5-Smad3 signaling pathway inhibits sprouting angiogenesis in the brain.

Mutation of *Tgfb1* and endothelial deletion of *Tgfbr2* or *Alk5* result in vascular sprouting, branching and hemorrhage

To identify the roles of specific TGFβ ligands *in vivo* responsible for the angiogenesis and hemorrhage phenotypes observed in *Itgb8ΔNE* mutants we examined *Tgfb1* and *Tgfb3* mutants. E14.5 *Tgfb1*$^{-/-}$ mutants exhibited brain hemorrhage throughout the neuroepithelium with associated glomeruloid vascular malformations (Fig. 5A). Similar to *Itgb8ΔNE* mutants, hemorrhage in *Tgfb1*$^{-/-}$ mice started in ventral brain regions at E12.5 (not shown) and progressed dorsally. When *Tgfb1*$^{-/-}$ telencephalic flat-mounts were examined, similar to *Itgb8ΔNE* mutants, we observed increases in vascular branch points, endothelial cell filopodia, vascular density and endothelial cell proliferation (Fig. 5B,D; supplementary material Fig. S4). We also observed pericyte detachment and proliferation (Fig. 5C) with a normal endothelial cell-to-pericyte ratio (not shown). By contrast, no angiogenic or hemorrhagic abnormalities were observed in *Tgfb3*$^{-/-}$ mutant forebrains (supplementary material Fig. S6). Consequently, TGFβ1 appears to be the most important ligand activated by integrin αVβ8 in the developing brain.

To further test the model that neuroepithelial cell αVβ8 activates TGFβ1, which suppresses endothelial cell sprouting and regulates

Development (2014) 141, 4489-4499 doi:10.1242/dev.107193

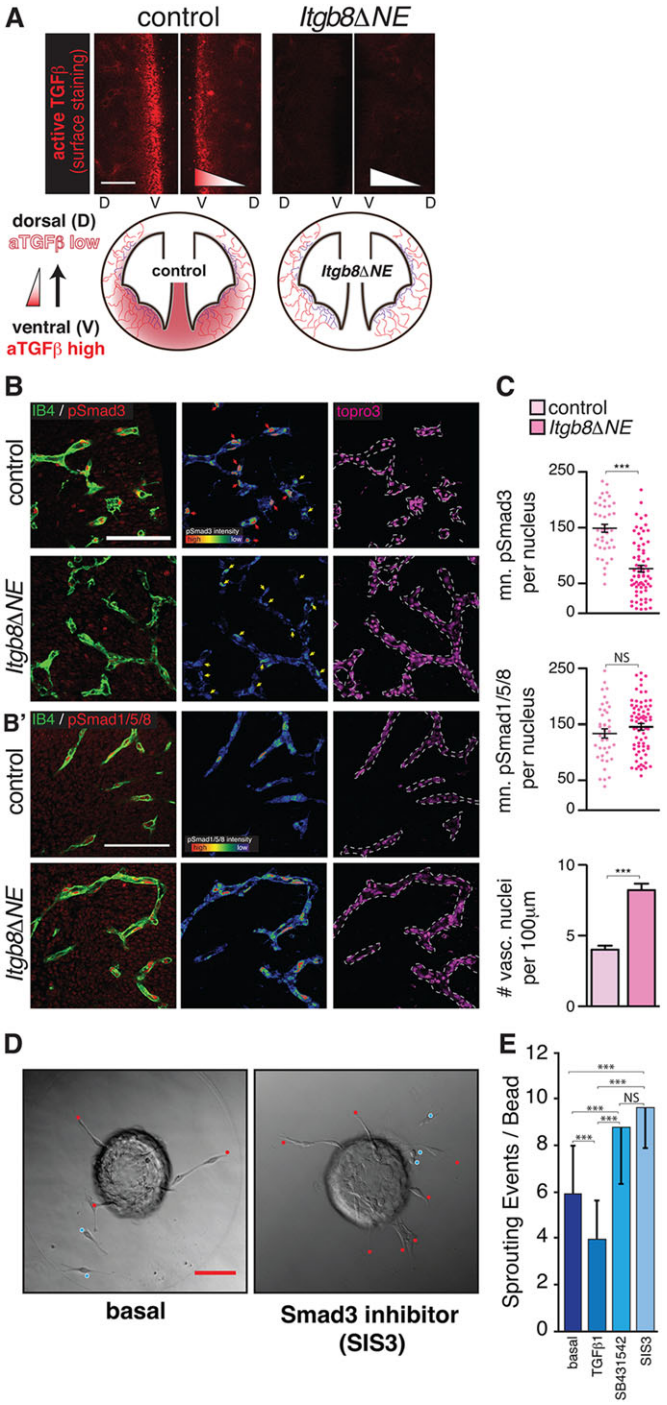

Fig. 4. Reduced active TGFβ and phosphorylated-Smad3 in mutant neuroepithelium and vasculature. (A) Surface expression at E11.5 of active TGFβ (aTGFβ, red) in control and mutant. In controls, active TGFβ levels are highest at the ventral midline (V). In mutants, active TGFβ levels are strikingly reduced. Schematic illustrates the distributions of active TGFβ in control and mutant at E11.5. (B,B′) Left panels: representative sections from E11.5 ventral midline region, illustrating (B) pSmad3 (red) or (B′) pSmad1/5/8 (red) colocalization with the endothelial marker IB4 (green) in control and mutant. Middle panels: intensity maps of pSmad within IB4-expressing cell nuclei (red is ~50-fold more intense than blue). There are significantly more vascular nuclei with high concentrations of pSmad3 (red arrows) in the controls than in mutants. Yellow arrows indicate vascular nuclei with low pSmad3. By contrast, there is no difference in the density of vascular nuclei expressing high pSmad1/5/8 in mutants versus controls. Right panels indicate TO-PRO-3-stained nuclei within the endothelium, as identified by IB4 labeling (dashed lines). (C) Quantification of pSmad3 and pSmad1/5/8 intensity within individual endothelial nuclei (arbitrary units) documents a significant reduction in vascular-specific pSmad3, but no change in pSmad1/5/8, in mutants versus controls. The number of vascular nuclei per unit vascular length is significantly increased, approximately twofold in the mutants. Error bars indicate s.e.m. *N*=4 controls, 4 mutants. (D) Representative images of MS-1 cell-coated beads cultured in fibrin gels under basal conditions (left) and in the presence of the Smad-3 inhibitor SIS3 (right). Sprouts (endothelial cells contacting bead, red dots) and scattered cells (endothelial cell sprouts not contacting bead, blue dots) represent individual sprouting events, quantified in E; *N*=81 (basal), 73 (TGFβ1), 56 (SB431542) and 59 (Sis3) total beads quantified. TGFβ1 results in reduced sprouting; the Smad3 inhibitor SIS3 or the more general TGFβ inhibitor SB431542 enhance sprouting. Values are mean±s.d. *P*-values from Student's *t*-test, ***$P<0.0001$. Scale bars: 100 µm.

vascular patterning, we generated an inducible endothelial cell-specific mutant (*Tgfbr2iΔEC*) by crossing *Tgfbr2*$^{floxed/floxed}$ and *Pdgfr-iCreERT2* mice (Claxton et al., 2008). To delete *Tgfbr2* when blood vessels first enter the CNS, tamoxifen was administered from E10.5 to E11.5 (Fig. 1A). When analyzed at E14.5 (Fig. 5A,B), mutant embryos exhibited severe brain hemorrhage with glomeruloid malformations (Fig. 5A). Recombination analysis using a Cre reporter revealed specific and efficient recombination within endothelial cells (not shown). Analysis of E12.5 telencephalic flat-mounts before hemorrhage (Fig. 5B,D; supplementary material Fig. S4) revealed vascular hypersprouting/hyperbranching, increased vascular density and endothelial cell proliferation similar to phenotypes in *Itgb8ΔNE* and *Tgfb1*$^{-/-}$ mutants. We also observed increased pericyte detachment and proliferation (Fig. 5C), similar to phenotypes seen in *Itgb8ΔNE* and *Tgfb1*$^{-/-}$ mutants. Consequently, the pericyte phenotypes observed in *Itgb8ΔNE* mutants are almost certainly indirect consequences of TGFβ signaling deficits in endothelial cells.

We then analyzed phenotypes of tamoxifen-induced endothelial cell-specific *Alk5* (Larsson et al., 2001) and *Alk1* mutants (Park et al., 2008). *Alk5iΔEC* mutants recapitulate the brain vascular and hemorrhage phenotypes observed in *Itgb8ΔNE*, *Tgfb1*$^{-/-}$ and *Tgfbr2iΔEC* mutants. There were no significant abnormalities in *Alk1iΔEC* mutants (supplementary material Fig. S6).

Finally, to determine whether TGFβ signaling in the neuroepithelium might contribute to these vascular phenotypes, we generated neuroepithelial cell-specific *Tgfbr2* mutants (*Tgfbr2ΔNE*). When analyzed at E12.5 (not shown) and E14.5 (supplementary material Fig. S6), mutants did not exhibit vascular malformations or hemorrhage. Consequently, the vascular malformations and hemorrhage must result from reduced TGFβ-TGFBR2-ALK5-Smad3 signaling within endothelial cells.

DISCUSSION

Our results argue that neuroepithelial cell-derived αVβ8 suppresses endothelial sprouting and maintains normal vascular patterning by activation of TGFβ1 and TGFBR2-ALK5-Smad3 signaling in endothelial cells, extending prior work (Arnold et al., 2012; Cambier et al., 2005; Nguyen et al., 2011) in several ways. Our prior analyses indicated that blood vessels exhibited defective initial invasion of the brain in the *Itgb8* mutant (Zhu et al., 2002). Our current time series analysis demonstrates that vessels ingress normally. Once vessels form the PVP, they hypersprout, hyperbranch and proliferate, then become more overtly dysplastic (glomeruloid) and hemorrhage. Vascular dysplasia and hemorrhage leads to retraction from the ventricular surface. Glomeruloid formation and hemorrhage are relatively late phenotypes, probably secondary to elevated sprouting, branching and proliferation of endothelial cells.

Development (2014) 141, 4489-4499 doi:10.1242/dev.107193

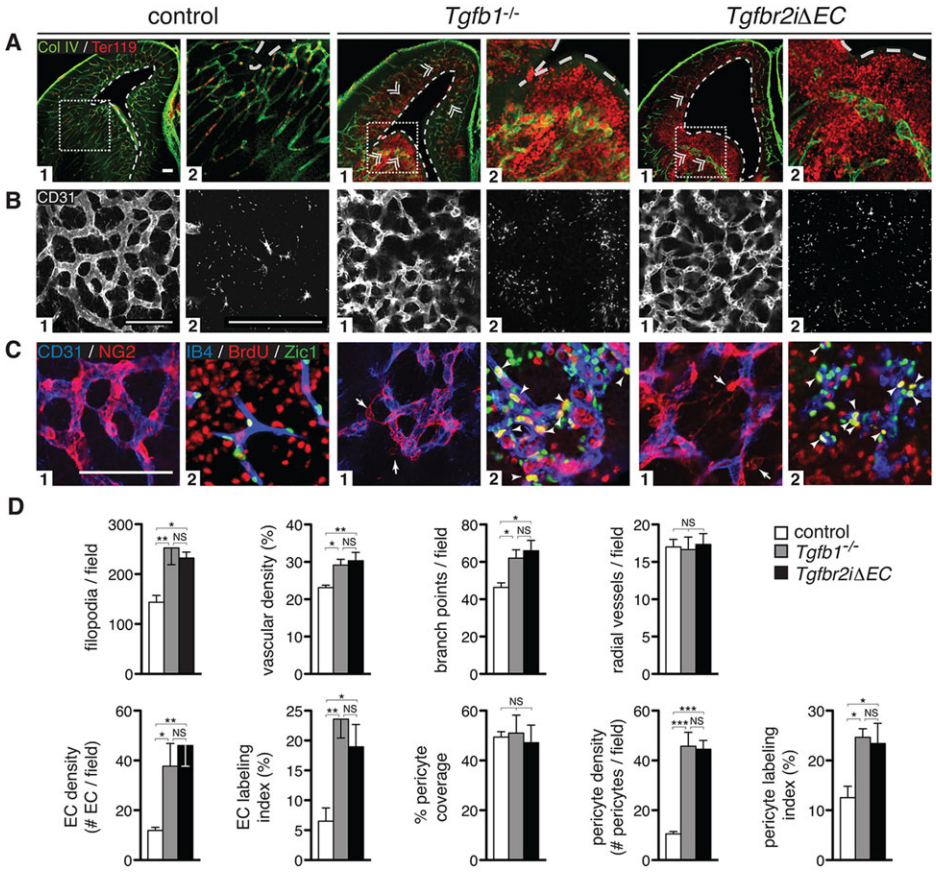

Fig. 5. Vascular hypersprouting and hemorrhage due to absence of TGFβ or endothelial cell-specific deletion of *Tgfbr2*. (A) E14.5 coronal forebrain sections. Labeling of vessels (Col IV, green) and red blood cells (Ter119, red) reveals diffuse hemorrhage and vascular malformations (glomeruloid bodies, double arrowheads) in *Tgfb1*$^{-/-}$ and endothelial cell-specific *Tgfbr2* (*Tgfbr2iΔEC*) mutants, but not in controls. A2 images are higher magnification insets of boxed regions. Note ventricular dilation (dotted white lines) in *Tgfb1*$^{-/-}$ and *Tgfbr2iΔEC* mutants versus controls. (B) Flat-mounts of telencephalon were stained for vessels (CD31, white) after which the PVP (B1) and brain parenchyma below containing filopodia (B2) were imaged (corresponding to levels 2 and 1, respectively, in Fig. 2A schematic). Images illustrate pronounced increases in vasculature, vascular branch point and filopodial densities in *Tgfb1*$^{-/-}$ and *Tgfbr2iΔEC* mutants. C1 images: Flat-mounts of telencephalon stained for endothelium (anti-CD31, blue) and pericytes (NG2, red). Panels reveal defects in association of pericytes with the vasculature in *Tgfb1*$^{-/-}$ and *Tgfbr2iΔEC* mutants. C2 images: Sections stained for pericyte nuclei (Zic1, green), proliferating cells (BrdU, red) and vessels (IB4, blue). Images reveal increased pericyte density and proliferation (arrowheads mark BrdU^{+}Zic1^{+} nuclei) in ventral brain regions of mutants. (D) Data quantification: Results show statistically significant increases in the number of filopodia/field, vascular density, vessel branch points/field, radial vessels/field and densities and proliferation of endothelial cells and pericytes in mutants. Vascular coverage with pericytes appears normal in each mutant versus controls (as described in Fig. 3; see also supplementary material Fig. S4). ANOVA *P*-values: **P*<0.05, ***P*<0.005, ****P*<0.0005; NS, not significant; *N*=8 (combined controls), *N*=4 (*Tgfb1*$^{-/-}$, *Tgfbr2iΔEC*). Error bars indicate s.e.m. Scale bars: 100 µm.

In addition to *Itgav* and *Itgb8*, brain hemorrhage during embryonic development is observed in other mutant mice, including *Gpr124* (Anderson et al., 2011; Cullen et al., 2011; Kuhnert et al., 2010), *Nrp1* (Gerhardt et al., 2004; Gu et al., 2003; Kawasaki et al., 1999), *Wnt7a/b-Bcat* (Daneman et al., 2009; Liebner et al., 2008; Stenman et al., 2008), *Tgfb1/3* (Mu et al., 2008), *Tgfbr2* (Nguyen et al., 2011; Robson et al., 2010), *Alk5* (Nguyen et al., 2011), *Smad4* (Li et al., 2011), *Smad2/Smad3* (Itoh et al., 2012) and *S1pr1* (Gaengel et al., 2012). Prior work either did not address the cause of hemorrhage (*Nrp1*, *Tgfb1/3*, *Smad2/Smad3*, *S1pr1*) or attributed it to a dysfunctional BBB [*Gpr124* (Anderson et al., 2011), *Bcat* (Liebner et al., 2008), *Smad4* (Li et al., 2011), *Itgb8* (Mobley et al., 2009), *Itgav-Tgfbr2-Alk5* (Nguyen et al., 2011)]. However, BBB dysfunction was generally tested by tracer injection after initiation of hemorrhage and thus did not determine whether BBB dysfunction precedes hemorrhage. We tested vascular barrier function in *Itgb8* mutants by tracer injection at time points when there was noticeable vascular pathology, but just prior to the onset of hemorrhage (E11.5). Surprisingly, we observed no detectable tracer leakage compared with pericyte-deficient mice, which have robust tracer leakage at this time (Armulik et al., 2010; Bell et al., 2010; Daneman et al., 2010) (Fig. 1). Additionally, pericyte-deficient mice have comparatively normal vascular morphogenesis without hemorrhage during initial cerebral angiogenesis. Thus, hemorrhage and BBB leakage are distinct processes. Due to the strong spatial-temporal association of sprouting abnormalities and brain hemorrhage, we propose that abnormal angiogenesis, not BBB dysfunction, causes brain hemorrhage.

We observed that vascular sprouting and patterning normally occur in a ventral-to-dorsal gradient, and that, in the absence of *Itgb8*, hypersprouting/-branching, glomeruloid formation and hemorrhage occurred in a similar gradient. These abnormalities were confined to tissue immediately adjacent to the cerebral ventricles; vessels further from the ventricles were not obviously affected. The selective sensitivity of PVP vessels is consistent with localized expression and/or activation of αVβ8-TGFβ signaling components. In parallel to these periventricular vascular gradients, we observed a similar gradation of activated TGFβ: high in ventral regions, low in dorsal regions. The loss of this gradient led to a commensurate reduction in

Development (2014) 141, 4489-4499 doi:10.1242/dev.107193

pSmad3 in PVP vessels. The concept that TGFβ1 forms a patterning gradient is consistent with reports showing that TGFβ superfamily members regulate patterning of diverse tissues during development (Wu and Hill, 2009). To our knowledge, we provide here the first description of TGFβ1 gradients in the brain, which direct the dorsal-ventral patterning of CNS vasculature.

Numerous reports describe an important role for TGFβ and BMP signaling in sprouting angiogenesis (Kim et al., 2012; Larrivée et al., 2012; Liu et al., 2009; Moya et al., 2012). However, the specific role of TGFβ1 in brain angiogenesis (vascular sprouting/branching) was previously unknown. Because global deletion of *Tgfb1* (and not *Tgfb3*), and endothelial cell-specific deletion of *Tgfbr2* or *Alk5* (and not *Alk1*), recapitulate the *Itgb8ΔNE* phenotype, loss of αVβ8-TGFβ1-TGFBR2-ALK5-Smad3 signaling is almost certainly responsible for vascular hypersprouting/hyperbranching, vascular glomeruloid formation and hemorrhage. BMP9/10-BMPR2-ALK1-Smad1/5/8 signaling, although present in developing CNS vessels, does not compensate for loss of αVβ8-TGFβ1-TGFBR2-ALK5-Smad3 signaling. The effects of αVβ8-TGFβ1 appear to be directed to endothelial cells, not the neuroepithelium, because endothelial cell-specific *Tgfbr2* and *Alk5* mutants phenocopy *Itgb8* mutants, and neuroepithelial cell-specific deletion of *Tgfbr2* exhibited no vascular phenotype. Consistent with this, it was recently shown that endothelial cell-specific *Smad2/Smad3* double mutants develop similar brain hemorrhage (Itoh et al., 2012). Although this report did not characterize brain vascular sprouting/branching, it is interesting to point out that *S1pr1* mRNA expression was downregulated in *Smad2/Smad3* mutants (Itoh et al., 2012), and endothelial cell-specific *S1pr1* mutants (like *Itgb8*, *Tgfb1*, *Tgfbr2* and *Alk5* mutants) develop endothelial cell hypersprouting before hemorrhage (Gaengel et al., 2012). It is now important to determine how αVβ8-TGFβ signaling interacts with other pathways, including VEGF, Notch, BMP and S1PR1, known to regulate sprouting angiogenesis.

Taken together, our findings show that disruption of αVβ8-TGFβ1-TGFBR2-ALK5-Smad3 signaling causes abnormal vascular sprouting and patterning, resulting in brain hemorrhage. Importantly, a similar pattern of brain hemorrhage and concurrent vascular dysplasia occurs in human infants with germinal matrix hemorrhage (GMH). In its most severe forms, GMH develops first with hemorrhage in ventral brain regions and then evolves to include dorsal/cortical regions (Volpe, 2009). Mirroring hemorrhage are gradients of endothelial cell density, proliferation and pro-angiogenic factors, such VEGF and ANGPT-2 (Ballabh et al., 2004a, 2007). Interestingly, CNS-specific VEGF overexpression was recently shown to cause vascular malformation and GMH in mice (Yang et al., 2013), and angiogenesis inhibitors that target VEGF reduce vascular proliferation and attenuate the severity of brain hemorrhage induced by hypertonic solution (Ballabh et al., 2007). Based on the similarities between infants with GMH and the *Itgb8/Tgfb* mutants, it will be important to determine how αVβ8-TGFβ1-TGFBR2-ALK5-Smad3 signaling might interface with VEGF-signaling and how these pathways might be altered in GMH.

MATERIALS AND METHODS

Mice

Itgb8$^{flox/flox}$ (Proctor et al., 2005), *Itgb8*$^{-/-}$ (Zhu et al., 2002; Arnold et al., 2012), *Pdgfb*$^{ret/ret}$ (Abramsson et al., 2003), *Tgfb1*$^{-/-}$ (Arnold et al., 2012), *Tgfb3*$^{-/-}$ (Proetzel et al., 1995), *Tgfbr2*$^{flox/flox}$ (Levéen et al., 2002), *Tgfbr1/Alk5*$^{flox/flox}$ (Larsson et al., 2001), *Tgfbr1/Alk1*$^{flox/flox}$ (Park et al., 2008), nesCre (nesCre8) (Petersen et al., 2002) and endothelial cell-specific *Pdgfb*iCreER^{TM2} mice (Claxton et al., 2008) have been described. To induce Cre activity, we administered 200 µl tamoxifen (15 mg/ml in corn oil) by oral gavage of pregnant dams for two days before embryo harvest. Embryonic stage (E) calculation defined the day following plug as E0.5. Mice were genotyped by PCR. Procedures were performed according to UCSF IACUC-approved guidelines. Experiments with *Pdgfb*$^{ret/ret}$ mice were approved by the local animal ethics committees in accordance with Swedish legislation.

Immunohistochemistry

Embryos at indicated time points were rinsed in PBS, fixed in ∼2 ml 4% paraformaldehyde (PFA) in PBS at 4°C overnight and stored at 4°C in PBS. Flat-mounted forebrains were embedded in 4% LM agarose in PBS (Sea Plaque Agarose, Cambex) and coronally sectioned at 450 µm using a vibratome. Forebrain thick sections and whole-dissected hindbrains were blocked in 1% BSA, 0.5% Triton X-100 in PBS (block buffer) overnight at 4°C, labeled with primary antibodies in block buffer overnight at 4°C and labeled with appropriate fluorophore-conjugated secondary antibodies in block buffer for 2 h at room temperature. Stained forebrain sections and hindbrains were flat-mounted in Prolong Gold (Invitrogen). Surface labeling of activated TGFβ was performed immediately after fixation in absence of Triton X-100. For thin sectioning, fixed brains were transferred to 30% sucrose in PBS overnight, embedded in OCT, then cryosectioned at 15 µm. Cryosections were permeabilized and blocked with 0.3% Triton X-100 and 3% BSA in PBS. Sections were incubated with primary antibodies overnight at 4°C, then with fluorophore-conjugated secondary antibodies (Invitrogen), TO-PRO-3 (Invitrogen) and mounted with Prolong Gold (Invitrogen). Whole-mount limb skin immunohistochemistry was performed as described (Li et al., 2013).

Antibodies

Primary antibodies: rat anti-CD31 (MEC13.3, BD Pharmingen, 550274; 1:100), goat anti-mouse CD31 (R&D Systems, AF3628; 1:100), rabbit anti-mouse Collagen IV (AbD Serotec, 2150-1470; 1:100), rat anti-mouse TER-119 (R&D Systems, MAB1125; 1:100), rabbit anti NG2 (W. Stallcup, Cancer Center, The Burnham Institute for Medical Research; 1:500), rabbit anti-Zic1 (Abcam, 72694; 1:50), rabbit anti-Erg (Abcam, 92513; 1:100), rabbit anti-pan-TGFβ (R&D Systems, AB-100NA; 1:100), rabbit anti-phospho-Smad3 (Epitomics, 1880-1; 1:100), rabbit anti-phospho-Smad 1/5/8 (Cell Signaling Technologies, 9511s; 1:100), mouse anti-rat nestin (4d4, AbD Serotec, 21263; 1:500), rabbit anti-brain lipid binding protein (BLBP) (Chemicon, AB9558; 1:500), rabbit anti-LYVE1 (Abcam, 14917; 1:100), rabbit anti-Nrp1 antibody (A. L. Kolodkin, Department of Neuroscience, Johns Hopkins University School of Medicine; 1:3000), mouse anti-BrdU (BD Biosciences; 1:50). Immunostaining with anti-Zic1 antibody used a Tyramide System Amplification (TSA) kit (Invitrogen) as per manufacturer's instructions. Pericyte specificity for Zic1 was demonstrated by lack of staining in pericyte-deficient mice (see Fig. 3C) (Daneman et al., 2010). Secondary antibodies: Alexa Fluor 488-, 555- or 647-conjugated donkey anti-rat, anti-rabbit, anti-goat or anti-mouse (Invitrogen).

Imaging

Confocal imaging was performed on a Zeiss LSM5 Pascal microscope.

BBB permeability

At E11.5, mutant and control mice were perfused by cardiac injection of Alexa Fluor 555-conjugated 70 kDa dextran (50 µl of 3.5 mg/ml in PBS; Invitrogen) using a pulled glass pipette with mouth connector and tubing (Sigma, P0799). Care was taken to ensure uniform rate of tracer delivery. Perfusion was confirmed by fluorescent visualization of the entire vascular system. Tracer circulated for 5 min at room temperature, embryos were decapitated, their heads fixed in 4% PFA overnight at 4°C and cryosectioned as described above.

Measurements

All measurements used high-resolution confocal images representing thin optical sections.

Development (2014) 141, 4489-4499 doi:10.1242/dev.107193

Morphometry

Calculations were made on brain flat-mounts. In the forebrain, the number of branch points and percentage area covered by CD31-positive endothelial cells were calculated from 460×460 µm fields using images taken from the PVP (level 2 in Fig. 2 schematic) in ventral regions (within medial and lateral ganglionic eminences; pink region in Fig. 2 schematic) or dorsal regions (immediately dorsal to medial and lateral ganglionic eminences; blue region in Fig. 2 schematic). $CD31^+$ radial vessel numbers were calculated from 460×460 µm fields using images superficial to the PVP (level 3 in Fig. 2 schematic). $CD31^+$ filopodia number was calculated from 230×230 µm fields using images taken deep to the PVP (level 1 in Fig. 2 schematic). Identical calculations were made in the hindbrain, except that ventro-medial regions (pink in schematic, supplementary material Fig. S3) were within alar and basal plates, and dorso-lateral regions (blue in schematic, supplementary material Fig. S3) were immediately dorso-lateral to these regions.

Pericyte coverage

NG2 and CD31 staining overlap was calculated from 460×460 µm fields using images taken from the PVP in ventral and dorsal regions as described (Abramsson et al., 2003).

Cell density and proliferation

Cell density was determined by averaging the number of Erg^+ endothelial nuclei or $Zic1^+$ pericyte nuclei per 40× image (230 µm×230 µm) field in at least four distinct fields as previously described (Siegenthaler et al., 2013). Pericyte:endothelial cell ratio (PC:EC) was calculated by dividing the average pericyte density by the average endothelial cell density. The cell proliferation index was calculated by dividing the number of $Erg^+/BrdU^+$ or $Zic1^+/BrdU^+$ nuclei by the number of Erg^+ or $Zic1^+$ nuclei in a 40× field.

Phospho-Smad immunofluorescent staining was quantified as described (Arnold et al., 2012).

Fibrin bead sprouting assay

mCherry-expressing microvascular endothelial (MS-1) cells were infected for 24 h with lentiviral particles (mCherry, Capital Biosciences) in MV2 medium (PromoCell) containing 5 µg/ml polybrene (Santa Cruz). MS-1 cells stably expressing mCherry were selected in the presence of 10 µg/ml puromycin (Invitrogen). The MS-1-mCherry fibrin bead assay was performed as previously described (Gaengel et al., 2012). A titration with TGFβ1 was used to select an optimal dose based on maximum phospho-Smad3 signal (supplementary material Fig. S5). Beads were cultured with 100 µl of basal MV2 medium in the presence or absence of recombinant TGFβ1 (10 ng/ml, Peprotech); TGFβ inhibitor SB431542 (3.5 µM, Sigma); Smad3 inhibitor SIS3 (10 µM, Calbiochem) for 6 days and scored for angiogenic sprouts (touching bead, red dots in Fig. 4D) and dissociated endothelial cells (not touching bead, blue dots in Fig. 4D). Previously published studies (Gaengel et al., 2012) revealed that endothelial cells form filopodia, sprout on the bead and then dissociate from the bead. Sprouts and dissociated cells were consequently tabulated together.

Biochemistry

Growth factor-starved MS-1 cells were stimulated with increasing concentrations of TGFβ1 (0-20 ng/ml) and frozen. For western blots, proteins were extracted and 10 mg of total proteins separated by SDS-PAGE, transferred to PVDF membranes before antibody application. For immunoprecipitation, cell and tissue lysates were clarified by centrifugation. Lysates were further precleared by protein G sepharose before incubation with antibody precoupled to protein G sepharose beads. Immunocomplexes were washed and separated by SDS-PAGE, transferred to nitrocellulose and blotted. Signals were detected using horseradish peroxidase-coupled secondary antibodies. For multiple probing, membranes were stripped and re-probed.

Statistics

P-values were defined using Student's *t*-test for paired comparisons and ANOVA for group-wise comparisons, with Tukey's post-hoc test analysis to compare individual groups. Four or more animals/samples were used for all experiments ($N \geq 4$). Controls for experiments with $Tgfb1^{-/-}$ and *Tgfbr2iΔEC* mice (see Fig. 5) were not significantly different in any parameter measured, and were therefore grouped together and used as a collective 'control'. Differences were considered significant with a $P<0.05$. Data are presented as mean±s.e.m.

Acknowledgements

We thank Ann Zovein, Rich Daneman, Hua Su and Steve Nishimura for discussions, and W. Stallcup and A. L. Kolodkin for generous gifts of antibodies.

Competing interests

The authors declare no competing financial interests.

Author contributions

T.D.A., C.N., M.-F.P., J.F., B.J., R.A., C.B., D.S., Y.M. and L.F.R. conceived and helped plan experiments. All authors, except C.B., D.S. and L.F.R., performed experiments. All authors helped analyze and evaluate data. T.D.A., C.B., D.S. and L.F.R. wrote the manuscript with critiques from all other authors.

Funding

Work was supported by Pediatric Critical Care Scientist Development Program K12HD047349 and Leducq Foundation Career Development Award (T.D.A.), NIH HL005702 (Y.M.), K99-R00 NS070920 (J.S.), Knut and Alice Wallenberg Foundation and European Research Council Advanced grant BBBARRIER (C.B.), 5R01 GM060514 and 5R01 HL078564 (R.A.), R37 HL53949 (D.S.), R01 NS19090 and Leducq Foundation Transatlantic Network of Excellence Award (L.F.R.). Deposited in PMC for release after 12 months.

Supplementary material

Supplementary material available online at
http://dev.biologists.org/lookup/suppl/doi:10.1242/dev.107193/-/DC1

References

Abramsson, A., Lindblom, P. and Betsholtz, C. (2003). Endothelial and nonendothelial sources of PDGF-B regulate pericyte recruitment and influence vascular pattern formation in tumors. *J. Clin. Invest.* **112**, 1142-1151.

Allinson, K. R., Lee, H. S., Fruttiger, M., McCarty, J. and Arthur, H. M. (2012). Endothelial expression of TGFβ type II receptor is required to maintain vascular integrity during postnatal development of the central nervous system. *PLoS ONE* **7**, e39336.

Anderson, K. D., Pan, L., Yang, X.-M., Hughes, V. C., Walls, J. R., Dominguez, M. G., Simmons, M. V., Burfeind, P., Xue, Y., Wei, Y. et al. (2011). Angiogenic sprouting into neural tissue requires Gpr124, an orphan G protein-coupled receptor. *Proc. Natl. Acad. Sci. USA* **108**, 2807-2812.

Armulik, A., Abramsson, A. and Betsholtz, C. (2005). Endothelial/pericyte interactions. *Circ. Res.* **97**, 512-523.

Armulik, A., Genové, G., Mäe, M., Nisancioglu, M. H., Wallgard, E., Niaudet, C., He, L., Norlin, J., Lindblom, P., Strittmatter, K. et al. (2010). Pericytes regulate the blood-brain barrier. *Nature* **468**, 557-561.

Arnold, T. D., Ferrero, G. M., Qiu, H., Phan, I. T., Akhurst, R. J., Huang, E. J. and Reichardt, L. F. (2012). Defective retinal vascular endothelial cell development as a consequence of impaired integrin αVβ8-mediated activation of transforming growth factor-β. *J. Neurosci.* **32**, 1197-1206.

Ballabh, P., Braun, A. and Nedergaard, M. (2004a). Anatomic analysis of blood vessels in germinal matrix, cerebral cortex, and white matter in developing infants. *Pediatr. Res.* **56**, 117-124.

Ballabh, P., Braun, A. and Nedergaard, M. (2004b). The blood-brain barrier: an overview: structure, regulation, and clinical implications. *Neurobiol. Dis.* **16**, 1-13.

Ballabh, P., Xu, H., Hu, F., Braun, A., Smith, K., Rivera, A., Lou, N., Ungvari, Z., Goldman, S. A., Csiszar, A. et al. (2007). Angiogenic inhibition reduces germinal matrix hemorrhage. *Nat. Med.* **13**, 477-485.

Bell, R. D., Winkler, E. A., Sagare, A. P., Singh, I., LaRue, B., Deane, R. and Zlokovic, B. V. (2010). Pericytes control key neurovascular functions and neuronal phenotype in the adult brain and during brain aging. *Neuron* **68**, 409-427.

Blanco, R. and Gerhardt, H. (2013). VEGF and notch in tip and stalk cell selection. *Cold Spring Harb. Perspect. Med.* **3**, a006569.

Braun, A., Xu, H., Hu, F., Kocherlakota, P., Siegel, D., Chander, P., Ungvari, Z., Csiszar, A., Nedergaard, M. and Ballabh, P. (2007). Paucity of pericytes in germinal matrix vasculature of premature infants. *J. Neurosci.* **27**, 12012-12024.

Cambier, S., Gline, S., Mu, D., Collins, R., Araya, J., Dolganov, G., Einheber, S., Boudreau, N. and Nishimura, S. L. (2005). Integrin alpha(v)beta8-mediated activation of transforming growth factor-beta by perivascular astrocytes: an angiogenic control switch. *Am. J. Pathol.* **166**, 1883-1894.

Development (2014) 141, 4489-4499 doi:10.1242/dev.107193

Claxton, S., Kostourou, V., Jadeja, S., Chambon, P., Hodivala-Dilke, K. and Fruttiger, M. (2008). Efficient, inducible Cre-recombinase activation in vascular endothelium. *Genesis* **46**, 74-80.

Corada, M., Nyqvist, D., Orsenigo, F., Caprini, A., Giampietro, C., Taketo, M. M., Iruela-Arispe, M. L., Adams, R. H. and Dejana, E. (2010). The Wnt/beta-catenin pathway modulates vascular remodeling and specification by upregulating Dll4/Notch signaling. *Dev. Cell* **18**, 938-949.

Cullen, M., Elzarrad, M. K., Seaman, S., Zudaire, E., Stevens, J., Yang, M. Y., Li, X., Chaudhary, A., Xu, L., Hilton, M. B. et al. (2011). GPR124, an orphan G protein-coupled receptor, is required for CNS-specific vascularization and establishment of the blood-brain barrier. *Proc. Natl. Acad. Sci. USA* **108**, 5759-5764.

Daneman, R., Agalliu, D., Zhou, L., Kuhnert, F., Kuo, C. J. and Barres, B. A. (2009). Wnt/beta-catenin signaling is required for CNS, but not non-CNS, angiogenesis. *Proc. Natl. Acad. Sci. USA* **106**, 641-646.

Daneman, R., Zhou, L., Kebede, A. A. and Barres, B. A. (2010). Pericytes are required for blood-brain barrier integrity during embryogenesis. *Nature* **468**, 562-566.

Fagiani, E. and Christofori, G. (2013). Angiopoietins in angiogenesis. *Cancer Lett.* **328**, 18-26.

Falk, S., Wurdak, H., Ittner, L. M., Ille, F., Sumara, G., Schmid, M.-T., Draganova, K., Lang, K. S., Paratore, C., Leveen, P. et al. (2008). Brain area-specific effect of TGF-beta signaling on Wnt-dependent neural stem cell expansion. *Cell Stem Cell* **2**, 472-483.

Freitas, C., Larrivée, B. and Eichmann, A. (2008). Netrins and UNC5 receptors in angiogenesis. *Angiogenesis* **11**, 23-29.

Gaengel, K., Niaudet, C., Hagikura, K., Laviña, B., Muhl, L., Hofmann, J. J., Ebarasi, L., Nyström, S., Rymo, S., Chen, L. L. et al. (2012). The sphingosine-1-phosphate receptor S1PR1 restricts sprouting angiogenesis by regulating the interplay between VE-cadherin and VEGFR2. *Dev. Cell* **23**, 587-599.

Gerhardt, H., Ruhrberg, C., Abramsson, A., Fujisawa, H., Shima, D. and Betsholtz, C. (2004). Neuropilin-1 is required for endothelial tip cell guidance in the developing central nervous system. *Dev. Dyn.* **231**, 503-509.

Gore, A. V., Swift, M. R., Cha, Y. R., Lo, B., McKinney, M. C., Li, W., Castranova, D., Davis, A., Mukouyama, Y.-S. and Weinstein, B. M. (2011). Rspo1/Wnt signaling promotes angiogenesis via Vegfc/Vegfr3. *Development* **138**, 4875-4886.

Gu, C., Rodriguez, E. R., Reimert, D. V., Shu, T., Fritzsch, B., Richards, L. J., Kolodkin, A. L. and Ginty, D. D. (2003). Neuropilin-1 conveys semaphorin and VEGF signaling during neural and cardiovascular development. *Dev. Cell* **5**, 45-57.

Hellström, M., Gerhardt, H., Kalén, M., Li, X., Eriksson, U., Wolburg, H. and Betsholtz, C. (2001). Lack of pericytes leads to endothelial hyperplasia and abnormal vascular morphogenesis. *J. Cell Biol.* **153**, 543-553.

Hirota, S., Liu, Q., Lee, H. S., Hossain, M. G., Lacy-Hulbert, A. and McCarty, J. H. (2011). The astrocyte-expressed integrin αvβ8 governs blood vessel sprouting in the developing retina. *Development* **138**, 5157-5166.

Itoh, F., Itoh, S., Adachi, T., Ichikawa, K., Matsumura, Y., Takagi, T., Festing, M., Watanabe, T., Weinstein, M., Karlsson, S. et al. (2012). Smad2/Smad3 in endothelium is indispensable for vascular stability via S1PR1 and N-cadherin expressions. *Blood* **119**, 5320-5328.

James, J. M., Gewolb, C. and Bautch, V. L. (2009). Neurovascular development uses VEGF-A signaling to regulate blood vessel ingression into the neural tube. *Development* **136**, 833-841.

Jinnin, M., Ihn, H. and Tamaki, K. (2006). Characterization of SIS3, a novel specific inhibitor of Smad3, and its effect on transforming growth factor-beta1-induced extracellular matrix expression. *Mol. Pharmacol.* **69**, 597-607.

Jung, B., Obinata, H., Galvani, S., Mendelson, K., Ding, B.-S., Skoura, A., Kinzel, B., Brinkmann, V., Rafii, S., Evans, T. et al. (2012). Flow-regulated endothelial S1P receptor-1 signaling sustains vascular development. *Dev. Cell* **23**, 600-610.

Kawasaki, T., Kitsukawa, T., Bekku, Y., Matsuda, Y., Sanbo, M., Yagi, T. and Fujisawa, H. (1999). A requirement for neuropilin-1 in embryonic vessel formation. *Development* **126**, 4895-4902.

Kim, J.-H., Peacock, M. R., George, S. C. and Hughes, C. C. W. (2012). BMP9 induces EphrinB2 expression in endothelial cells through an Alk1-BMPRII/ActRII-ID1/ID3-dependent pathway: implications for hereditary hemorrhagic telangiectasia type II. *Angiogenesis* **15**, 497-509.

Kuhnert, F., Mancuso, M. R., Shamloo, A., Wang, H.-T., Choksi, V., Florek, M., Su, H., Fruttiger, M., Young, W. L. and Heilshorn, S. C. (2010). Essential regulation of CNS angiogenesis by the orphan G protein-coupled receptor GPR124. *Science* **330**, 985-989.

Larrivée, B., Prahst, C., Gordon, E., del Toro, R., Mathivet, T., Duarte, A., Simons, M. and Eichmann, A. (2012). ALK1 signaling inhibits angiogenesis by cooperating with the Notch pathway. *Dev. Cell* **22**, 489-500.

Larsson, J., Goumans, M. J., Sjöstrand, L. J., van Rooijen, M. A., Ward, D., Levéen, P., Xu, X., ten Dijke, P., Mummery, C. L. and Karlsson, S. (2001). Abnormal angiogenesis but intact hematopoietic potential in TGF-beta type I receptor-deficient mice. *EMBO J.* **20**, 1663-1673.

Levéen, P., Larsson, J., Ehinger, M., Cilio, C. M., Sundler, M., Sjöstrand, L. J., Holmdahl, R. and Karlsson, S. (2002). Induced disruption of the transforming growth factor beta type II receptor gene in mice causes a lethal inflammatory disorder that is transplantable. *Blood* **100**, 560-568.

Li, J., Qu, X., Yao, J., Caruana, G., Ricardo, S. D., Yamamoto, Y., Yamamoto, H. and Bertram, J. F. (2010). Blockade of endothelial-mesenchymal transition by a Smad3 inhibitor delays the early development of streptozotocin-induced diabetic nephropathy. *Diabetes* **59**, 2612-2624.

Li, F., Lan, Y., Wang, Y., Wang, J., Yang, G., Meng, F., Han, H., Meng, A., Wang, Y. and Yang, X. (2011). Endothelial Smad4 maintains cerebrovascular integrity by activating N-cadherin through cooperation with Notch. *Dev. Cell* **20**, 291-302.

Li, W., Kohara, H., Uchida, Y., James, J. M., Soneji, K., Cronshaw, D. G., Zou, Y.-R., Nagasawa, T. and Mukouyama, Y.-S. (2013). Peripheral nerve-derived CXCL12 and VEGF-A regulate the patterning of arterial vessel branching in developing limb skin. *Dev. Cell* **24**, 359-371.

Liebner, S., Corada, M., Bangsow, T., Babbage, J., Taddei, A., Czupalla, C. J., Reis, M., Felici, A., Wolburg, H., Fruttiger, M. et al. (2008). Wnt/beta-catenin signaling controls development of the blood-brain barrier. *J. Cell Biol.* **183**, 409-417.

Liu, Y., Wada, R., Yamashita, T., Mi, Y., Deng, C.-X., Hobson, J. P., Rosenfeldt, H. M., Nava, V. E., Chae, S.-S., Lee, M.-J. et al. (2000). Edg-1, the G protein–coupled receptor for sphingosine-1-phosphate, is essential for vascular maturation. *J. Clin. Invest.* **106**, 951-961.

Liu, Z., Kobayashi, K., van Dinther, M., van Heiningen, S. H., Valdimarsdottir, G., van Laar, T., Scharpfenecker, M., Löwik, C. W.G. M., Goumans, M.-J., Ten Dijke, P. et al. (2009). VEGF and inhibitors of TGFbeta type-I receptor kinase synergistically promote blood-vessel formation by inducing alpha5-integrin expression. *J. Cell Sci.* **122**, 3294-3302.

McCarty, J. H., Monahan-Earley, R. A., Brown, L. F., Keller, M., Gerhardt, H., Rubin, K., Shani, M., Dvorak, H. F., Wolburg, H., Bader, B. L. et al. (2002). Defective associations between blood vessels and brain parenchyma lead to cerebral hemorrhage in mice lacking alphav integrins. *Mol. Cell. Biol.* **22**, 7667-7677.

McCarty, J. H., Lacy-Hulbert, A., Charest, A., Bronson, R. T., Crowley, D., Housman, D., Savill, J., Roes, J. and Hynes, R. O. (2005). Selective ablation of alphav integrins in the central nervous system leads to cerebral hemorrhage, seizures, axonal degeneration and premature death. *Development* **132**, 165-176.

Melton, A. C., Bailey-Bucktrout, S. L., Travis, M. A., Fife, B. T., Bluestone, J. A. and Sheppard, D. (2010). Expression of αvβ8 integrin on dendritic cells regulates Th17 cell development and experimental autoimmune encephalomyelitis in mice. *J. Clin. Invest.* **120**, 4436-4444.

Mobley, A. K., Tchaicha, J. H., Shin, J., Hossain, M. G. and McCarty, J. H. (2009). Beta8 integrin regulates neurogenesis and neurovascular homeostasis in the adult brain. *J. Cell Sci.* **122**, 1842-1851.

Moya, I. M., Umans, L., Maas, E., Pereira, P. N. G., Beets, K., Francis, A., Sents, W., Robertson, E. J., Mummery, C. L., Huylebroeck, D. et al. (2012). Stalk cell phenotype depends on integration of Notch and Smad1/5 signaling cascades. *Dev. Cell* **22**, 501-514.

Mu, Z., Yang, Z., Yu, D., Zhao, Z. and Munger, J. S. (2008). TGFbeta1 and TGFbeta3 are partially redundant effectors in brain vascular morphogenesis. *Mech. Dev.* **125**, 508-516.

Nguyen, H.-L., Lee, Y. J., Shin, J., Lee, E., Park, S. O., McCarty, J. H. and Oh, S. P. (2011). TGF-β signaling in endothelial cells, but not neuroepithelial cells, is essential for cerebral vascular development. *Lab. Invest.* **91**, 1554-1563.

Nitta, T., Hata, M., Gotoh, S., Seo, Y., Sasaki, H., Hashimoto, N., Furuse, M. and Tsukita, S. (2003). Size-selective loosening of the blood-brain barrier in claudin-5-deficient mice. *J. Cell Biol.* **161**, 653-660.

Pardali, E., Goumans, M.-J. and ten Dijke, P. (2010). Signaling by members of the TGF-beta family in vascular morphogenesis and disease. *Trends. Cell Biol.* **20**, 556-567.

Park, S. O., Lee, Y. J., Seki, T., Hong, K.-H., Fliess, N., Jiang, Z., Park, A., Wu, X., Kaartinen, V., Roman, B. L. et al. (2008). ALK5- and TGFBR2-independent role of ALK1 in the pathogenesis of hereditary hemorrhagic telangiectasia type 2. *Blood* **111**, 633-642.

Petersen, P. H., Zou, K., Hwang, J. K., Jan, Y. N. and Zhong, W. (2002). Progenitor cell maintenance requires numb and numblike during mouse neurogenesis. *Nature* **419**, 929-934.

Phng, L.-K. and Gerhardt, H. (2009). Angiogenesis: a team effort coordinated by notch. *Dev. Cell* **16**, 196-208.

Proctor, J. M., Zang, K., Wang, D., Wang, R. and Reichardt, L. F. (2005). Vascular development of the brain requires beta8 integrin expression in the neuroepithelium. *J. Neurosci.* **25**, 9940-9948.

Proetzel, G., Pawlowski, S. A., Wiles, M. V., Yin, M., Boivin, G. P., Howles, P. N., Ding, J., Ferguson, M. W. J. and Doetschman, T. (1995). Transforming growth factor-beta 3 is required for secondary palate fusion. *Nat. Genet.* **11**, 409-414.

Robson, A., Allinson, K. R., Anderson, R. H., Henderson, D. J. and Arthur, H. M. (2010). The TGFβ type II receptor plays a critical role in the endothelial cells during cardiac development. *Dev. Dyn.* **239**, 2435-2442.

Ruhrberg, C., Gerhardt, H., Golding, M., Watson, R., Ioannidou, S., Fujisawa, H., Betsholtz, C. and Shima, D. T. (2002). Spatially restricted patterning cues provided by heparin-binding VEGF-A control blood vessel branching morphogenesis. *Genes Dev.* **16**, 2684-2698.

Sawamiphak, S., Seidel, S., Essmann, C. L., Wilkinson, G. A., Pitulescu, M. E., Acker, T. and Acker-Palmer, A. (2010). Ephrin-B2 regulates VEGFR2 function in developmental and tumour angiogenesis. *Nature* **465**, 487-491.

Shoham, A. B., Malkinson, G., Krief, S., Shwartz, Y., Ely, Y., Ferrara, N., Yaniv, K. and Zelzer, E. (2012). S1P1 inhibits sprouting angiogenesis during vascular development. *Development* **139**, 3859-3869.

Siegenthaler, J. A., Choe, Y., Patterson, K. P., Hsieh, I., Li, D., Jaminet, S.-C., Daneman, R., Kume, T., Huang, E. J. and Pleasure, S. J. (2013). Foxc1 is required by pericytes during fetal brain angiogenesis. *Biol. Open* **2**, 647-659.

Stenman, J. M., Rajagopal, J., Carroll, T. J., Ishibashi, M., McMahon, J. and McMahon, A. P. (2008). Canonical Wnt signaling regulates organ-specific assembly and differentiation of CNS vasculature. *Science* **322**, 1247-1250.

Takashima, S. and Tanaka, K. (1978). Development of cerebrovascular architecture and its relationship to periventricular leukomalacia. *Arch. Neurol.* **35**, 11-16.

Vasudevan, A., Long, J. E., Crandall, J. E., Rubenstein, J. L. R. and Bhide, P. G. (2008). Compartment-specific transcription factors orchestrate angiogenesis gradients in the embryonic brain. *Nat. Neurosci.* **11**, 429-439.

Volpe, J. J. (2009). Brain injury in premature infants: a complex amalgam of destructive and developmental disturbances. *Lancet Neurol.* **8**, 110-124.

Walls, J. R., Coultas, L., Rossant, J. and Henkelman, R. M. (2008). Three-dimensional analysis of vascular development in the mouse embryo. *PLoS ONE* **3**, e2853.

Wang, Y., Nakayama, M., Pitulescu, M. E., Schmidt, T. S., Bochenek, M. L., Sakakibara, A., Adams, S., Davy, A., Deutsch, U., Lüthi, U. et al. (2010). Ephrin-B2 controls VEGF-induced angiogenesis and lymphangiogenesis. *Nature* **465**, 483-486.

Wang, Y., Rattner, A., Zhou, Y., Williams, J., Smallwood, P. M. and Nathans, J. (2012). Norrin/Frizzled4 signaling in retinal vascular development and blood brain barrier plasticity. *Cell* **151**, 1332-1344.

Wu, M. Y. and Hill, C. S. (2009). Tgf-beta superfamily signaling in embryonic development and homeostasis. *Dev. Cell* **16**, 329-343.

Yamazaki, S., Ema, H., Karlsson, G., Yamaguchi, T., Miyoshi, H., Shioda, S., Taketo, M. M., Karlsson, S., Iwama, A. and Nakauchi, H. (2011). Nonmyelinating Schwann cells maintain hematopoietic stem cell hibernation in the bone marrow niche. *Cell* **147**, 1146-1158.

Yang, Z., Mu, Z., Dabovic, B., Jurukovski, V., Yu, D., Sung, J., Xiong, X. and Munger, J. S. (2007). Absence of integrin-mediated TGFbeta1 activation in vivo recapitulates the phenotype of TGFbeta1-null mice. *J. Cell Biol.* **176**, 787-793.

Yang, D., Baumann, J. M., Sun, Y.-Y., Tang, M., Dunn, R. S., Akeson, A. L., Kernie, S. G., Kallapur, S., Lindquist, D. M., Huang, E. J. et al. (2013). Overexpression of vascular endothelial growth factor in the germinal matrix induces neurovascular proteases and intraventricular hemorrhage. *Sci. Transl. Med.* **5**, 193ra90.

Yu, B. P., Yu, C. C. and Robertson, R. T. (1994). Patterns of capillaries in developing cerebral and cerebellar cortices of rats. *Acta Anat.* **149**, 128-133.

Zhu, J., Motejlek, K., Wang, D., Zang, K., Schmidt, A. and Reichardt, L. F. (2002). beta8 integrins are required for vascular morphogenesis in mouse embryos. *Development* **129**, 2891-2903.